TURBOMACHINERY & PUMP SYMPOSIA | HOUSTON, TX
SEPTEMBER 13-15, 2022
SHORT COURSES: SEPTEMBER 12, 2022

VISUALIZATION OF OIL-WATER EMULSION FORMATION IN A CENTRIFUGAL PUMP STAGE

Rodolfo Marcilli Perissinotto
Ph.D. Candidate in Mechanical Engineering
University of Campinas (UNICAMP)
Campinas, Sao Paulo, Brazil

Rafael Franklin Lazaro de Cerqueira
Post-Doc Researcher
University of Campinas (UNICAMP)
Campinas, Sao Paulo, Brazil

William Monte Verde
Researcher Scientist
University of Campinas (UNICAMP)
Campinas, Sao Paulo, Brazil

Jorge Luiz Biazussi
Researcher Scientist
University of Campinas (UNICAMP)
Campinas, Sao Paulo, Brazil

Antonio Carlos Bannwart
Professor
University of Campinas (UNICAMP)
Campinas, Sao Paulo, Brazil

Marcelo Souza de Castro
Professor
University of Campinas (UNICAMP)
Campinas, Sao Paulo, Brazil

Rodolfo Marcilli Perissinotto is a doctoral student in mechanical engineering with emphasis in thermal and fluids at the School of Mechanical Engineering (FEM) at the University of Campinas (UNICAMP). Member of Artificial Lift & Flow Assurance (ALFA) research group with activities in the Center for Energy and Petroleum Studies (CEPETRO). Currently participating of Energy Production Innovation Center (EPIC), research project sponsored by Equinor Brazil and São Paulo Research Foundation (FAPESP). Master of science in mechanical engineering in 2018 at UNICAMP, with six years of experience in flow visualization, centrifugal pumps, multiphase flows, and related topics.

Rafael Franklin Lazaro de Cerqueira is a post-doctoral researcher at ALFA/CEPETRO. He holds a doctorate (2020) and a master's degree (2015) in mechanical engineering from the Federal University of Santa Catarina, in Brazil. His main topic of interest is the field of multiphase flows. He has experience with the experimental characterization of multiphase flows using the PIV (Particle Image Velocimetry) and PTV (Particle Tracking Velocimetry) techniques and development of digital imaging, deep learning and computer vision tools aimed for the analysis of multiphase flows. He also has experience with CFD (Computational Fluid Dynamics) modeling of multiphase flows.

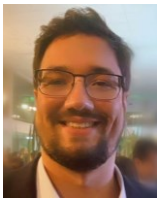

William Monte Verde is a researcher at ALFA/CEPETRO since 2017. In recent years, he has been technical manager of several research projects related to energy companies and also has worked at EPIC, sponsored by Equinor Brazil and FAPESP. In addition, he has provided consulting services to oil and gas companies, both operators and service providers. Master of science in mechanical engineering in 2010 and doctorate in science and petroleum engineering in 2014, both at UNICAMP. His interests include multiphase flow and turbomachines, mainly on the following topics: visualization techniques, multiphase flow modeling, pumps operating with viscous fluids and two-phase flows.

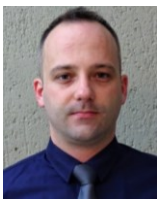

Jorge Luiz Biazussi has been a researcher at ALFA/CEPETRO for 8 years. Former technical coordinator of EPIC, in research lines related to electrical submersible pump (ESP), emulsions, two-phase flows and optimization of production systems. In recent years, he has provided consulting services to oil and gas companies, both operators and service providers. Master of science in mechanical engineering in 2010 and doctorate in science and petroleum engineering in 2014, both at UNICAMP. He completed a specialization course in Applied and Strategic Project Management in 2020 and he is currently taking another course in Strategic Management of Technological Innovation at UNICAMP. He has recently joined Baker Hughes as Lead Service Specialist, Artificial Lift Systems, Oilfield Services.

ABSTRACT

Electrical submersible pumps are assembled in oil wells to act as artificial lift methods. When water is present in the reservoir, oil-water emulsions are formed in the pump. These two-phase mixtures affect the performance and promote instabilities that lead the machine to operate inefficiently and fail prematurely. Therefore, this paper aims to investigate the formation of emulsions and behavior of mineral oil drops in a transparent centrifugal pump through a flow visualization approach. Shut-off, best efficiency point, and open-flow conditions are investigated at three impeller rotational speeds with high-speed imaging and particle image velocimetry. As the oil fraction increases, large drops accumulate in the impeller channels, while some escape to the volute and circulate until the water flow carries them out of the pump stage. Regions with vortices and water recirculation explain the accumulation of oil drops in the impeller and reduced pump performance at low water flow rates. Intense velocity fluctuations at the impeller and impeller-volute boundary indicate the main causes for oil drop rotation, deformation, and fragmentation at high water flow rates. The new findings can be used to improve models and numerical simulations for pumps operating with multiphase flows and help the creation of new pump designs.

1. INTRODUCTION

In the oil production chain, the use of artificial lift methods is important to ensure acceptable flow rates and reasonable costs. This fact is mainly valid for mature fields where the reservoir usually has insufficient energy to expel the fluids naturally and for heavy oil fields where the fluids often have high viscosities which impair the recovery rate. In both cases, artificial lift techniques vertically transport the fluids stored in the reservoir, through the well to the surface facilities, compensating for pressure loss caused by friction and gravity.

In this context, the electrical submersible pump (ESP) stands out as one of the most relevant equipment used for artificial lifting. The ESP is responsible for 10% of the oil supply (Takacs, 2017) as it has been installed in more than 150,000 oil wells in the world (Flatern, 2015). The ESP is indeed a robust and flexible device, capable of working in hostile environments, in onshore or offshore wells worldwide (Bremner *et al*., 2006). Nevertheless, the operation of an ESP sometimes involves some problems which are still a challenge for engineers and technicians.

Most of these malfunctions are related to the characteristics of the fluid being pumped. As an ESP essentially consists of a multistage centrifugal pump, the device is very effective in pumping incompressible and low-viscous fluids, such as single-phase water. However, the ESP often faces operational issues when it works with complex multiphase flows typically found in oil production. The presence of a compressible gaseous phase containing the lightest oil fractions, or even a viscous liquid-liquid emulsion containing connate or injected water, leads the pump to experience efficiency losses in addition to operational instabilities with the potential of reducing the production rates and the system lifetime.

In practical terms, as the global economic activities demand 100 million barrels of oil a day (U.S. Energy Information Administration, 2021), any inefficiencies in the operation of pumps have the effect of incurring financial losses to companies from the oil and gas sector. In view of this scenario, the scientific community has been using flow visualization methods to improve the understanding on physical phenomena that occur in single-phase and two-phase flows in pump impellers and diffusers (Perissinotto *et al*., 2021) to investigate their relationship with the pump behavior and performance.

The literature on single-phase flows is very extensive. Some authors have been using particle image velocimetry (PIV) techniques (Raffel *et al*., 2007) to characterize the flow in components of pumps operating with water (e.g. Pedersen *et al*., 2003; Krause *et al*., 2006; Keller *et al*., 2014; Li *et al*., 2020; Shi *et al*., 2021). With regard to gas-liquid flows, many authors have used high-speed imaging (HSI) to identify flow patterns, evaluate the dependence of pump performance on gas volume fraction, and determine when the surging and gas locking events normally occur (e.g. Monte Verde *et al*., 2017; Morrison *et al*., 2017; Shao *et al*., 2018; Stel *et al*., 2019; Mansour *et al*., 2019; Cubas *et al*., 2020; Zhao *et al*., 2021), for example.

However, within the scope of liquid-liquid flows, there is an evident lack of published research on flow visualization. A few authors have used microscopes (e.g. Bulgarelli *et al*., 2020a, 2020b) or endoscopes (e.g. Valdés *et al*., 2020; Schmitt *et al*., 2021) to characterize emulsions and complement studies on effective viscosity and phase inversion, while other authors adopted techniques based on laser diffraction and ultrasound (e.g. Ibrahim and Maloka, 2006; Morales *et al*., 2012) to obtain drop diameter distributions. However, these measurements are usually conducted outside the impeller, from fluid samples extracted from the pump, or in regions such as the pump inlet and outlet. As a consequence, these studies are not able to investigate the formation of emulsions or the behavior of dispersed drops within the pump stage. The visualization of individual drops moving inside an ESP stage is incipient and it has been achieved only by Perissinotto *et al*. (2019, 2020) for oil-water (o/w) and water-oil (w/o) dispersions.

Therefore, this paper aims to expand the visualization of dispersions in centrifugal pumps. The objective is to characterize the transient process of an o/w emulsion formation, in order to investigate drop breaking mechanisms and to identify possible flow patterns in moving and stationary pump parts. To achieve this task, single- and two-phase flow tests were carried out with a transparent pump prototype, a HSI equipment, and a PIV system. A technique based on particle tracking velocimetry (PTV) was also adopted to track individual drops and manually calculate their velocities.

The present study contributes to the literature by generating a knowledge basis on the behavior and dynamics of two-phase mixtures in ESP impellers. These advancements are very important for the validation of numerical simulations focused on complex flows. Such simulations nowadays use turbulence flow models that cannot fully reproduce the real phenomena that take place in turbomachines. In addition, the observations performed with flow visualization methods are essential for the proposition or improvement of mathematical models that predict the pressure increment or represent the dynamics of dispersed drops in pumps.

In fact, the results achieved in this study have recently been used in the development of an effective viscosity model (Bulgarelli *et al*., 2021). Other practical applications are expected in the near future. In a long-term horizon, understanding the motion of single- and two-phase flows in impellers may be useful for designing more efficient pumps capable of preventing or delaying the formation of undesirable o/w and w/o emulsions.

2. METHODS AND PROCEDURES

The experimental program adopted in this paper can be divided into: 1) Developing a new pump prototype and assembling a new test facility (section 2.1); 2) Performing experiments (section 2.2); 3) Processing data and images (section 2.3) to obtain results.

2.1 Experimental Facility

A transparent centrifugal pump prototype was manufactured with the objective of allowing flow visualization in its impeller, whose design is based on a real ESP model. The radial impeller has seven channels, a constant height of 6 mm, an eye diameter of 44 mm and an outer diameter of 110 mm. The top cover (shroud) and the blades are made of polished acrylic, while the bottom cover (hub) is made of anodized aluminum. Besides, the impeller is assembled in the space between two flat plates joined by screws and nuts, where a spiral volute was machined. Thus, the prototype has a vaneless volute instead of a multi-vaned diffuser. The decision to use the volute in the pump design aimed to facilitate the entry of light into the pump stage during the visualization experiments.

As depicted in Fig. 1, the prototype is installed in a test bench with tanks, pumps, valves, and a visualization system with camera and laser, which are the main components of HSI and PIV methods. This apparatus was assembled to enable the injection of continuous and dispersed phases into the transparent pump. According to information available in Perissinotto *et al*. (2022), the first liquid (continuous phase) enters the impeller through four inlet ports assembled on the side of the pump body. The second liquid (dispersed phase), in turn, is introduced through a hollow central shaft. When this second liquid reaches the shaft extremity, it passes through a radial component that has seven symmetrically spaced holes. As highlighted in Fig. 1, these holes uniformly divide the flow and inject the second liquid into the entrance of each impeller channel, promoting the formation of a two-phase mixture.

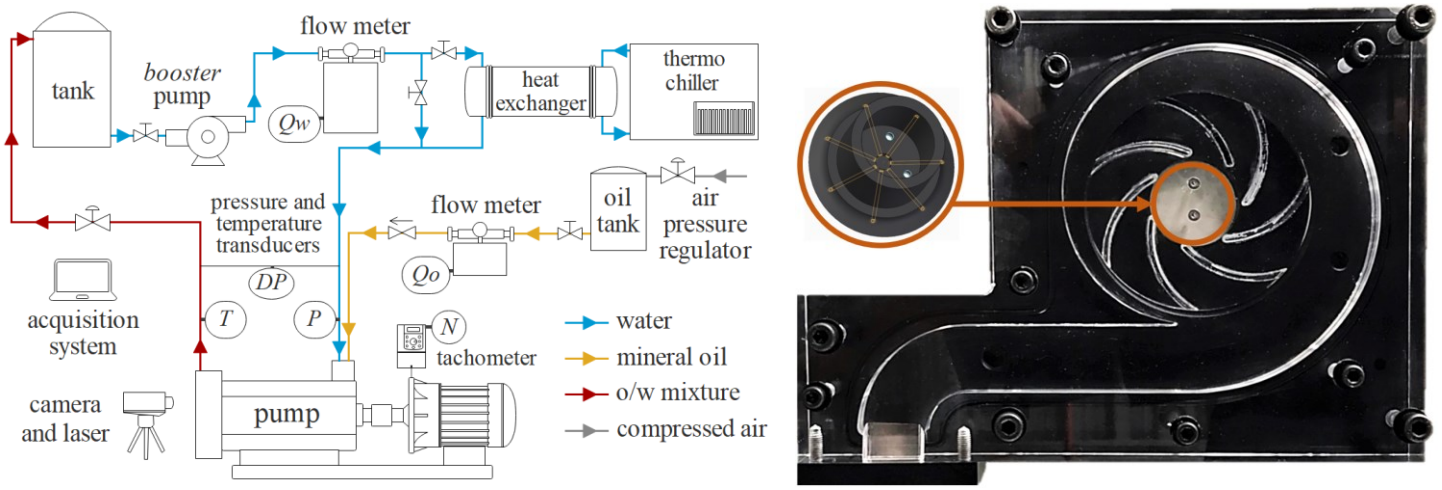

Fig. 1 - Illustrative drawing of the test facility (left) and photograph of the pump stage with transparent parts (right). The highlighted component injects and distributes the dispersed phase into the entrance of the impeller channels.

Only the water circuit (blue) is operated in the single-phase flow tests. In this case, the booster pump circulates tap water, which passes through the flowmeter and heat exchanger, reaches the pump prototype, and finally returns to the main tank. However, during two-phase flow tests, the oil injection system (yellow) is used together with the water circuit. The pressure regulator injects air into the oil tank, which forces the mineral oil to move at a desired flow rate measured by the other flowmeter. Then, an oil-water mixture is formed inside the pump, and flow visualization is performed. When this mixture (red) leaves the pump, it flows to the main tank, where both fluids are naturally separated by density differences.

Five instruments measure the impeller rotational speed (N), water flow rate (Qw), oil flow rate (Qo), absolute pressure at pump inlet (P), differential pressure generated by the pump (DP), as well as the flow temperature in the pump outlet (T). The temperature of both fluids is approximately equal to the ambient temperature, i.e., around 20ºC. Uncertainties are lower than 0.5% of the measured values. The experimental setup followed the Hydraulic Institute Standards for configuration and instrumentation. However, additional instruments were included in the facility to measure DP in different positions of the transparent pump, as this type of data is important to the development of models and pump designs. These positions are presented in section 3.1 together with performance curves.

These performance curves were obtained for single-phase water flow. In the tests, the rotational speed is set by a variable speed driver (VSD) installed at the pump motor, while the water flow rate is controlled by a valve installed at the pump outlet. By manipulating the

driver, a different N is obtained, and the pump head curve changes. By opening or closing the valve, the system curve or total dynamic head (TDH) is modified, so a different Qw is obtained. This procedure allows the analysis of different operating points.

Furthermore, by controlling the booster pump, the pressure at the transparent pump inlet is kept at a constant value P = 0.5 bar during the experiments. This value ensures that the net positive suction head (NPSH) is sufficiently high to prevent cavitation. In other words, the NPSHA is higher than the NPSH3. As the pump operates without the presence of gases, this inlet pressure does not affect the density of the mixture, which is composed of two incompressible liquids.

2.2 Experimental Program

The experiments executed in this research included two-phase oil-water flow tests with the HSI method at different pump operating conditions (Part I). Then, some of these tests were repeated with a single-phase water flow and the PIV technique to further characterize the continuous phase (Part II).

Part I - Two-Phase Oil-Water Flow

A high-speed camera was used as flow visualization method in the two-phase flow tests. The images acquired with this device have a dimension of 2560 x 1600 pixels at the maximum acquisition rate of 1400 fps. In this case, two different mineral oils were used as dispersed phase: Oil I has a density ρ_{o_1} = 880 kg/m³ and viscosity μ_{o_1} = 220 cP, while Oil II has ρ_{o_2} = 860 kg/m³ and μ_{o_2} = 20 cP at the ambient temperature in the laboratory. For a comparison, water has ρ_w = 999 kg/m³ and μ_w = 1 cP at the same temperature. These oils have also been lightened with a white dye, in a 0.5% mass concentration, to enhance contrast with the dark background on the images. The dye did not influence ρ and μ. Four types of analyses were performed:

1 – Oil I, N = 300 rpm, Qw = 0 kg/h (shut-off), Qo_1 = 0.5 g/s, until the camera memory was full of images;
2 – Oil II, N = 300 rpm, Qw = 0 kg/h (shut-off), Qo_2 = 2.5 g/s, until the emulsion impaired the visualization;
3 – Oil II, N = 300 rpm, Qw = 750 kg/h ≈ 200 g/s (best efficiency point) and Qw = 1100 kg/h ≈ 300 g/s (open-flow), Qo_2 = 2.5 g/s;
4 – Oil II, N = 600 rpm and N = 900 rpm, Qw = 150 kg/h ≈ 40 g/s (close to shut-off), Qo_2 = 5.0 g/s, until the camera memory was full.

According to the information above, the experiments were performed at the BEP, but also at shut-off and open-flow. Although these two last conditions are extreme and unlikely for a real ESP in the field, it may be interesting to investigate them, as they are associated with a flow behavior that would present the most significant differences in relation to the design point.

Another important observation is related to the liquid-liquid dispersion analyzed in this paper, which is oil-water type. Although the w/o emulsion (water dispersed in oil) is the most usual emulsion pumped by an ESP, the o/w emulsion (oil dispersed in water) sometimes occurs in real cases, especially in situations in which the inversion point is low.

Part II - Single-Phase Water Flow

A time-resolved PIV system was adopted to visualize single-phase flows. The equipment has a laser generator that provides an energy of 30 mJ per pulse when operating at 1 kHz repetition rate. Mirrors and lenses were adjusted so the laser plane illuminated the center of the impeller with a thickness of 2 mm. Microspheres of acrylic doped with rhodamine were added to the water to act as tracers. Each experiment consists of acquiring 500 pairs of flow images with the impeller at a fixed position. This procedure ensures that the channels and blades are always at a constant angular position, defined by an angular encoder, thus the average velocity fields and derived quantities can be properly computed. Two analyses were carried out:

5 – N = 300 rpm, Qw = 0 kg/h, Qw = 750 kg/h and Qw = 1100 kg/h, for a comparison with items 1, 2, 3.
6 – N = 600 rpm and N = 900 rpm, Qw = 150 kg/h, for a comparison with item 4.

2.3 Image and Data Processing

A few HSI images of the two-phase flow were processed using a PTV method. A sample of individual oil drops were tracked through a manual approach in the camera control software, which determined the position (R, θ) and velocity ($\vec{V}$) of these drops as a function of time (t). The procedure is similar to the one adopted by Perissinotto *et al*. (2019, 2020). The drop velocity has radial (V_R) and circumferential (V_θ) components in a fixed polar coordinate system with its origin at the center of the impeller:

$$\vec{V} = V_R\,\hat{\imath}_R + V_\theta\,\hat{\imath}_\theta = \dot{R}\,\hat{\imath}_R + R\dot{\theta}\,\hat{\imath}_\theta \tag{1}$$

A new PTV approach based on convolutional neural networks was also developed by Cerqueira *et al*. (2022). This image processing technique is currently being used by them to track oil drops on the HSI images acquired in the present paper. The main objective is to automatize the tracking procedure in the near future, in order to study a large population of oil drops, without manual efforts.

In regard to the single-phase water flow, in turn, the PIV images were processed in a commercial software. Algorithms were developed and used to: 1) Remove the impeller motion from the images; 2) Apply masks to define the region of interest; 3) Apply filters to improve quality and reduce noise; 4) Compute the instantaneous velocity fields through a cross-correlation method; 5) Calculate the ensemble-averaged velocities and derived quantities; and 6) Interpolate the results to obtain smooth graphical representations. Such procedure was inspired in the recent studies by Tielicke and Sonntag (2021) and Liu *et al*. (2021).

The procedure is able to provide the instantaneous and also the average relative velocity ($\vec{u}$) without considering the angular component due to the impeller rotation. The result is similar to tracking the tracer particles in a non-inertial coordinate system that moves jointly with the impeller. When necessary, the angular term proportional to the impeller angular speed and radial position (ωR) can be added back to $\vec{u}$ for an estimation of the average absolute velocity ($\vec{U}$) as well. This last velocity is related to an inertial fixed frame of reference:

$$\vec{U} = \vec{u} + \vec{\omega} \times \vec{R} \tag{2}$$

Velocity fluctuations (u') are also extracted from the PIV images. The fluctuations represent the difference between the instantaneous and average velocities of the water flow. These quantities are essential for the evaluation of the turbulence levels in the pump.

3. RESULTS AND DISCUSSIONS

The following paragraphs describe and discuss the pump performance (section 3.1) and the main observations and results obtained from the visualization of two-phase o/w dispersions (section 3.2) and single-phase water flow (section 3.3) in the transparent pump stage.

3.1 Pressure Increment as a function of Flow Rate

As mentioned in section 2.1, the transparent pump has different static pressure measurement points, which allow an analysis of the static pressure gain in various positions. Examples of *DP* x *Qw* curves for single-phase water flow at *N* = 300 rpm are available below in Fig. 2. As observed, *DP21* represents the pressure between the volute exit (discharge) and the pump body near the water entrance (suction); *DP22* symbolizes the pressure between the volute exit and the impeller inlet (pump stage); *DP12* then indicates the pressure between the impeller outlet and inlet (impeller channel).

As can be noticed, the point Pi_2 is connected to the mechanism that was originally designed to inject and distribute the dispersed phase into the impeller channels. This injection system was exceptionally used to measure the pressure Pi_2 because the experiments conducted in the current section are single-phase flow, i.e., it was not necessary to inject a second liquid into the system during the tests.

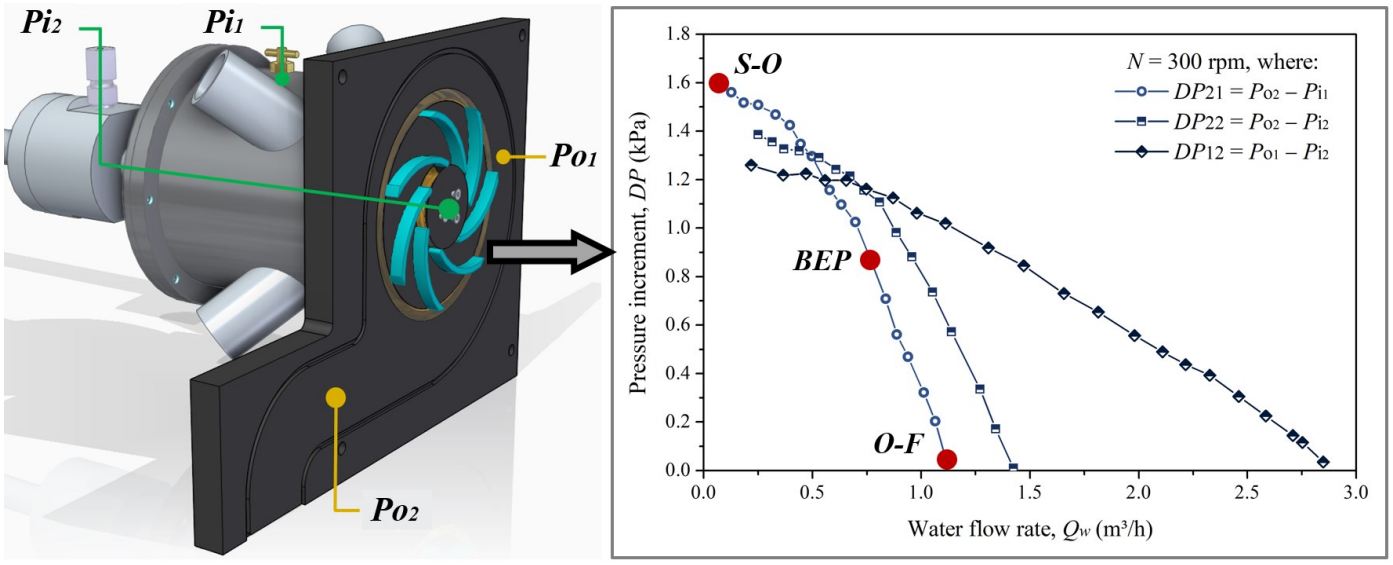

Fig. 2 - Illustrative drawing of the static pressure measurement positions (left) and graph with static pressure increment curves (right) for single-phase water flow. The impeller rotates at 300 rpm.

The pressure increment *DP21* is frequently used in the pump head calculation. Hence, the shut-off (S-O), best efficiency point (BEP) and open-flow (O-F) were highlighted in the *DP21* curve. These three conditions are further investigated in the next sections with a flow visualization approach. The BEP was previously defined, in commissioning tests, from measurements conducted with a torquemeter.

Similar curves were obtained for *N* = 600 rpm and *N* = 900 rpm. Parameters such as dimensionless head and flow rate were calculated and compared. The dynamic similarity was assured at the three rotational speeds investigated in this manuscript. At *N* = 600 rpm, the BEP occurs at *Qw* = 1500 kg/h and *DP21* = 4.2 kPa. At *N* = 900 rpm, it corresponds to *Qw* = 2200 kg/h and *DP21* = 9.8 kPa.

3.2 Visualization of Two-phase Oil-water Mixtures

The first condition simulated is the shut-off, in which the water flow is *Qw* = 0, but the mineral oil continues to be injected. Examples of images captured at this condition are available in Fig. 3 as a function of the instant of time (*t*) after the start of oil injection. In Fig. 3a, Oil I (more viscous) was added to water at a Qo_1 = 0.5 g/s = 1.8 kg/h flow rate. Then, in Fig. 3b, Oil II (less viscous) was added at Qo_2 = 2.5 g/s = 9.0 kg/h to compose the o/w dispersion. In both cases, the mass of water in the pump stage is constant and approximately

Mw = 0.2 kg, since the internal volume of the pump stage (impeller + volute) is about 0.2 liter. At the same time, the total mass of oil injected in the pump, Mo, increases with t, so the mass fraction $\lambda = Mo / Mw$ gradually increases too. The impeller rotates clockwise at N = 300 rpm and, as explained above, the oil drops appear white in the images because they have been dyed to enhance contrast with the dark background.

An evident accumulation of large drops can be identified inside the impeller channels. These drops are practically stationary, as if they were stuck in the impeller. Thus, it is understood that drag and other forces are insufficient to carry these drops out of the impeller. The effect is intensified by the difference in densities between the continuous (water, ρ_w = 1000 kg/m³) and dispersed ($860 < \rho_o < 880$ kg/m³) phases. In other words, the centrifugal acceleration tends to act more intensely on water than on oil, a fact that would favor the accumulation of oil drops. A slip between both phases is expected as well.

The drops that remain in the impeller rarely deform or break up. The drops which manage to escape the impeller finish fragmenting at the impeller-volute boundary, characterized by substantial velocity differences between the rotating impeller and stationary volute. In addition, as the water flow rate is zero, these oil drops remain inside the pump stage, where they keep circulating and breaking up in the volute spiral. Near the exit region of the pump stage, it is observed that the volute tongue "pulls" the drops back to the beginning of the volute, probably as an effect of velocity gradients (Keller *et al*., 2014). This behavior favors the formation of emulsions as time passes.

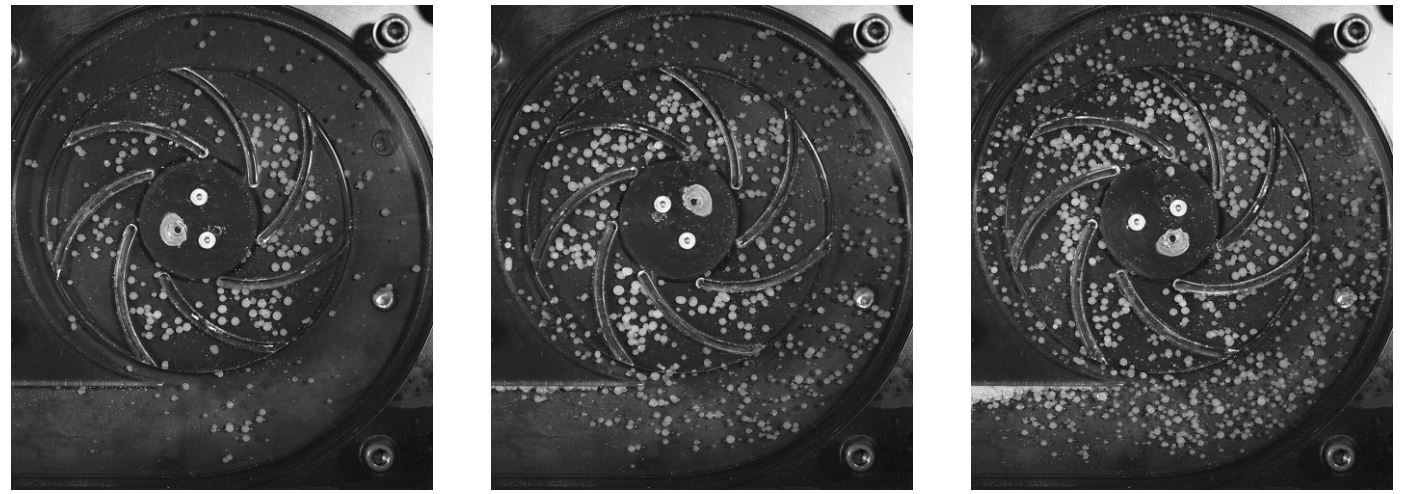

Line a) Oil I, t = 3.0 s, λ = 0.8% | Oil I, t = 7.0 s, λ = 1.8% | Oil I, t = 12.0 s, λ = 3.0%

Line b) Oil II, t = 3.0 s, λ = 3.8% | Oil II, t = 5.0 s, λ = 6.2% | Oil II, t = 7.0 s, λ = 8.8%

Fig. 3 - Flow images acquired at N = 300 rpm and Qw = 0 kg/h (0.0 Q_{BEP}) with injection of two different mineral oils.

The next analyses are focused on Oil II. Still at N = 300 rpm, the second and third flow rates investigated are Qw = 750 kg/h and Qw = 1100 kg/h, equivalent to the BEP and open-flow, respectively. Examples of flow images are available in Fig. 4. In these cases, there is no accumulation of drops in the impeller because the water flow rate is sufficiently large to drag them out of the pump stage. The flow rate ratio $\beta = Qo / Qw$ ranges between 0.8% and 1.2%.

At the BEP, the drops enter the impeller in the form of jets due to the oil injector mechanism, and soon they assume a spherical or elliptical shape. As can be noticed, the dispersed drops are evenly distributed, indicating that the continuous phase is well-behaved, as expected for a centrifugal pump working at the BEP (Li *et al*., 2020). The breakage events are less frequent now, but they still occur, mainly at the impeller outlet and the volute tongue. Besides, some drops still circulate in the volute before leaving the stage, but this fact is probably not observed in a real ESP as it usually has vaned diffusers instead of vaneless volutes.

There are no visual differences between the BEP and open-flow conditions regarding the size of the oil drops. However, at the open-flow, the oil drops move closer to the pressure blades, suggesting that the water velocity profile is more irregular when compared with the BEP. In this configuration in which the continuous phase has a higher flow rate, a few drops enter and stay at the gap between the impeller shroud and the front visualization window. This fact confirms that there is probably some water flowing in this region as well.

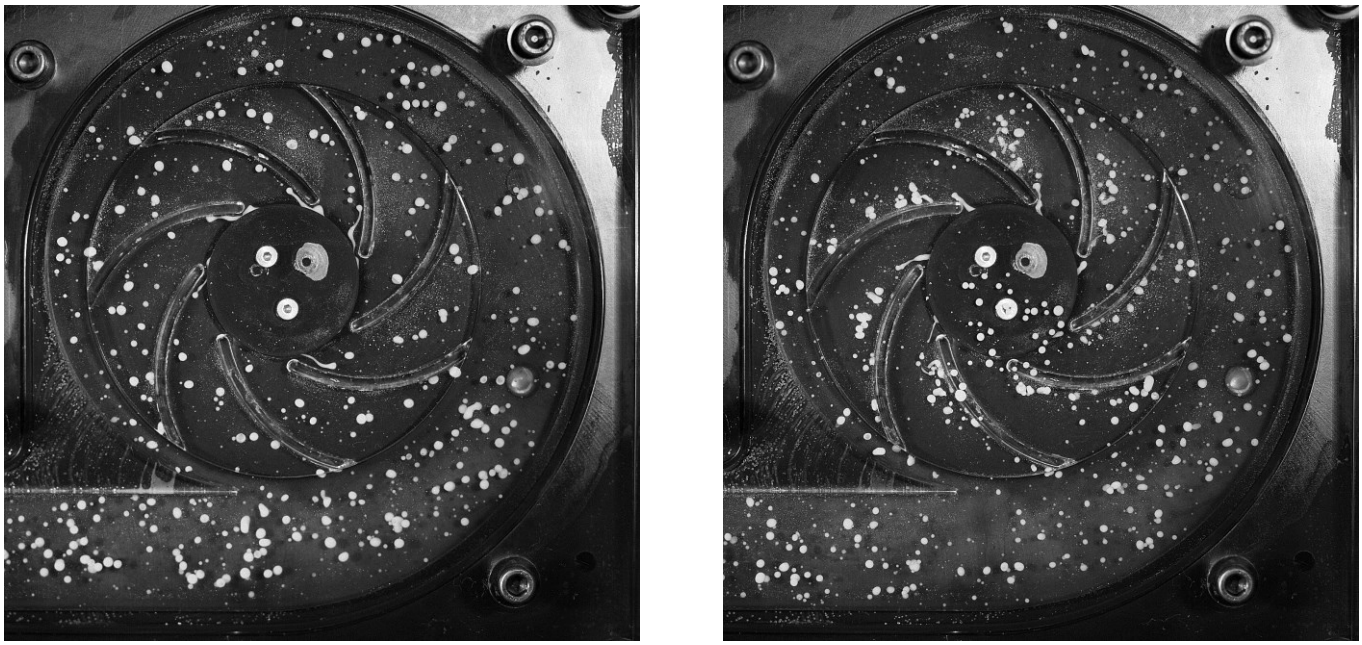

Qw = 750 kg/h (1.0 Q_{BEP}), β = 1.2% Qw = 1100 kg/h (1.5 Q_{BEP}), β = 0.8%

Fig. 4 - Flow images acquired with water and Oil II at N = 300 rpm and Qo_2 = 2.5 g/s.

For N = 300 rpm, Qw = 750 kg/h (1.0 Q_{BEP}) and Qo_2 = 2.5 g/s (Oil II), three drops were manually tracked so that their motion in the pump stage could be investigated. Figure 5 shows the image obtained in the camera control software after the end of the tracking process, which lasted for almost 900 frames, or 0.90 seconds. As can be observed, the three oil drops consist of one mother-drop that breaks up into two daughter-drops during its trajectory. Figure 5 also shows the velocities as a function of time, where the blue, green, and yellow curves refer respectively to the drops described above. The radial velocity magnitude (V_R, solid lines) is lower than the circumferential velocity magnitude (V_θ, dashed lines). The polar frame of reference indicates that R increases radially outward while θ increases in the counterclockwise direction, therefore V_R tends to be positive and V_θ tends to be negative. The impeller moves clockwise.

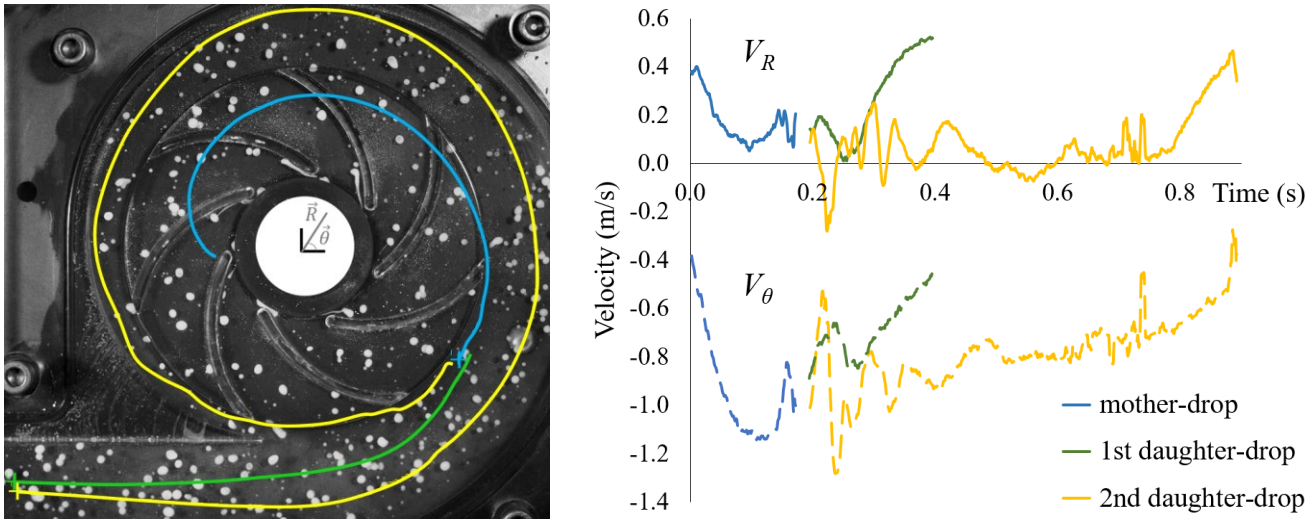

Fig. 5 - Kinematics of three oil drops tracked in the pump: trajectory (left) and velocity curves (right).

The mother-drop (blue path), which practically remains only in the impeller, receives an angular velocity proportional to the impeller rotational speed and radius. The first daughter-drop (green path) goes directly to the pump exit, while the second daughter-drop (yellow path), in turn, circulates the volute more than 450° (1 ¼ rotation) with minimum displacements in the radial direction.

The mother-drop takes 0.17 seconds to traverse the channel. When leaving the impeller and entering the volute, this drop undergoes a deformation due to shear stresses related to intense velocity differences in the region. Then, the drop breaks up into two daughter-drops, in a process that requires 0.02 seconds, illustrated in Fig. 6. After the fragmentation, as stated above, one of the new drops goes directly to the pump exit, in a displacement that lasts 0.20 seconds. The other daughter-drop remains in the impeller-volute boundary region for 0.05 seconds, as shown in Fig. 7. This daughter-drop is dragged back to the beginning of the spiral and then it performs a circular motion throughout the volute. The displacement lasts 0.52 seconds, until the drop exits the pump stage.

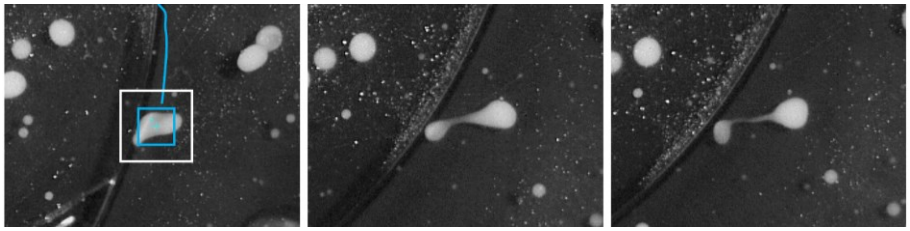

Fig. 6 - Mother-drop breaking up into two new daughter-drops.

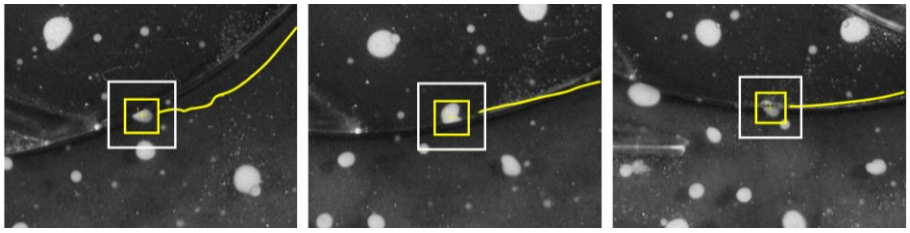

Fig. 7 - Daughter-drop moving next to the impeller-volute boundary region.

At N = 600 rpm and N = 900 rpm, with flow rates Qw = 150 kg/h and Qo_2 = 5.0 g/s = 18.0 kg/h, the accumulation of oil drops in the impeller is observed again. The phenomenon is similar to that identified at 300 rpm. However, as the rotational speeds are higher, the oil drops now appear smaller in the images, due to more frequent fragmentation events as a consequence of more intense forces in the pump stage. Examples of images at various instants of time (t) are shown in Fig. 8 and Fig. 9. The flow rate ratio $\beta = Qo / Qw$ is 12.0%.

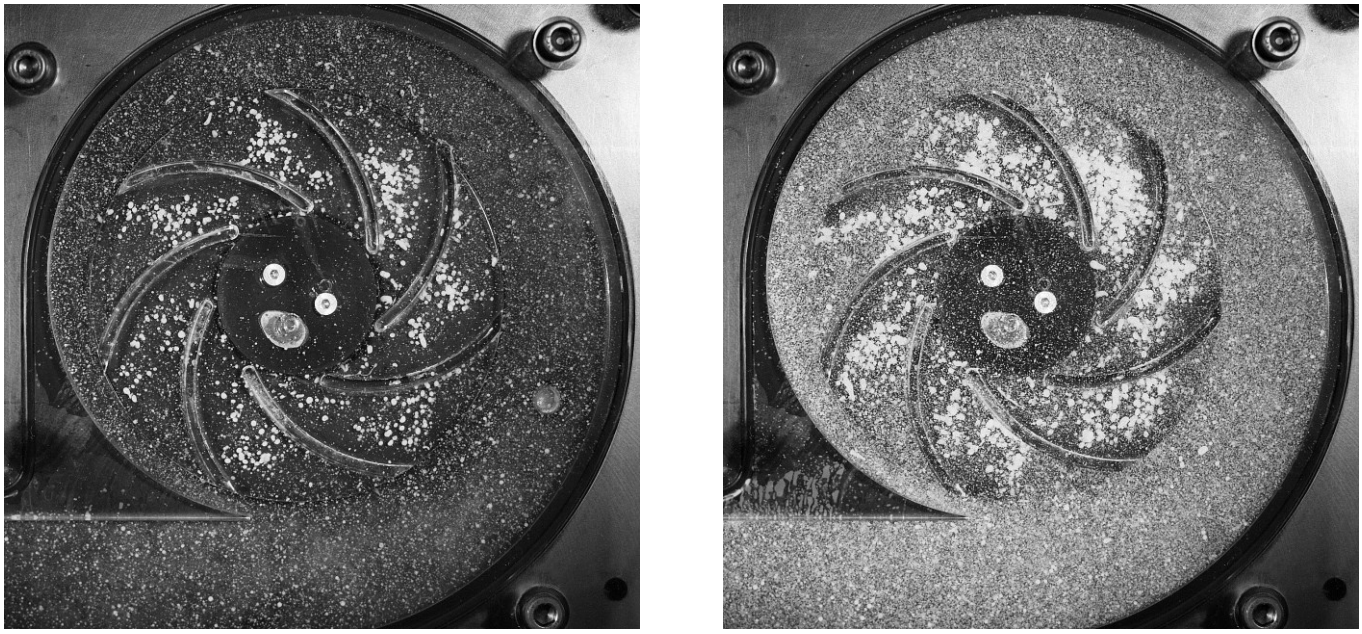

t = 1.0 s t = 5.0 s

Fig. 8 - Flow images acquired with Oil II, at N = 600 rpm, Qw = 150 kg/h (0.10 Q_{BEP}), Qo_2 = 5.0 g/s, β = 12.0%.

Although the water flow rate (Qw) is 8 times greater than the oil injection rate (Qo), many drops keep circulating in the volute before leaving the pump stage. In this situation, these drops enter and leave the impeller several times, in an intermittent movement, which intensifies the breakage of the dispersed phase at the boundary region between impeller and volute. Hence, in both rotations, the complete formation of an o/w emulsion occurs after about 10 seconds. At that moment, the transient tests must be finished, because it becomes impossible to distinguish the tiny drops in the images. The flow becomes turbid to the point where it is no longer possible to visualize the background of the pump stage.

t = 0.5 s t = 2.5 s

Fig. 9 - Flow images acquired with Oil II, at N = 900 rpm, Qw = 150 kg/h (0.08 Q_{BEP}), Qo_2 = 5.0 g/s, β = 12.0%.

As a supplementary material, videos that complement the analysis are available at a YouTube channel. They can be accessed via this link: *www.youtube.com/playlist?list=PLO0Nr4bWIQyQ6FuzX3f0Le8SE4lyZnLSy*. A QR Code was also added to Fig. 9 for the reader's convenience.

3.3 Influence of Continuous Phase on Dispersed Phase

The experiments executed with the PIV method resulted in the velocity fields depicted in Fig. 10 for N = 600 rpm and Qw = 150 kg/h. In Fig. 10a, the average velocity $\vec{u}$ was calculated in a rotative frame of reference, as if the observer rotates together with the impeller, while, in Fig. 10b, the velocity $\vec{U}$ was computed in a fixed coordinate system, including the volute as well. Thus, the difference between both velocity fields is essentially the presence or absence of the term proportional to the impeller angular speed and radius (ωR). As can be noted, the PIV vectors were plotted overlaid on HSI images captured after t = 0.5 s from the start of Oil II injection at Qo_2 = 5.0 g/s in the pump stage.

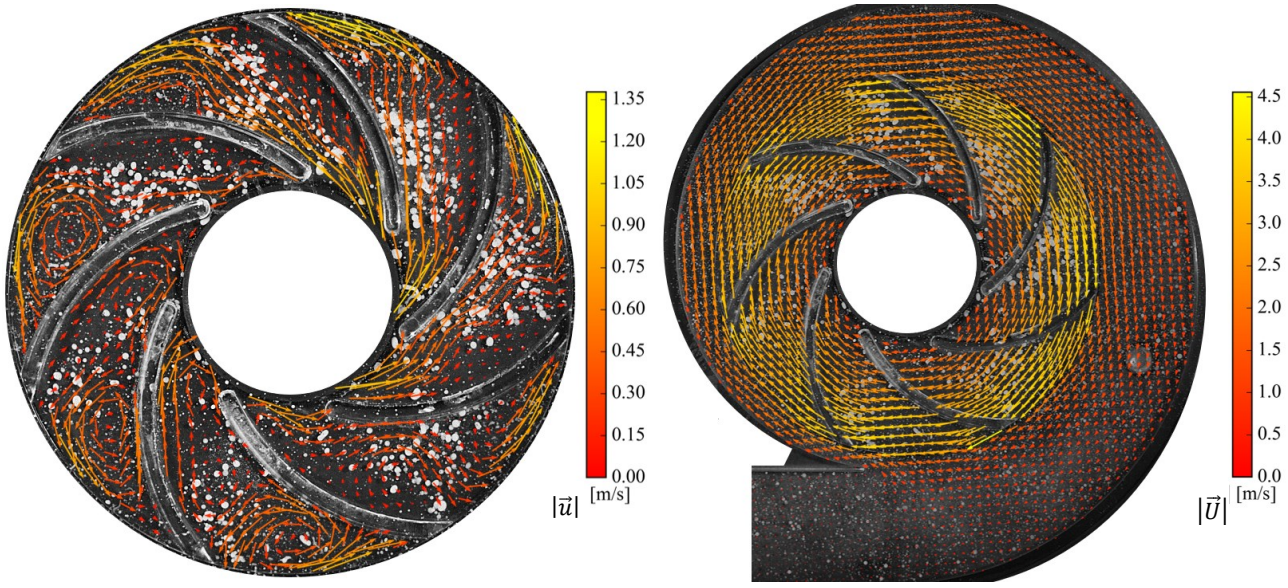

(a) Relative water velocity in the impeller. (b) Absolute water velocity in the entire stage.

Fig. 10 - Average water velocity fields at N = 600 rpm and Qw = 150 kg/h (0.10 Q_{BEP}) plotted over two-phase flow images captured with presence of Oil II at Qo_2 = 5.0 g/s, i.e., β = 12.0%.

As seen in Fig. 10a, the water velocity field (single-phase) is congruent with the movement of dispersed oil drops (two-phase flow). Inside the channels, the drops tend to move in regions where the water velocity is higher. In places with lower water velocities, in turn, the presence of drops is unusual. The same observation is valid for recirculation zones, with occurrence of vortices that rotate clockwise and counterclockwise (Krause *et al*., 2006), for example. The images thus indicate that the characteristics of the water flow would affect the behavior and motion of the oil drops in the pump impeller.

Then, in Fig. 10b, water velocity has the highest magnitude at the impeller outlet, as an effect of the rotational speed at the outer radius. However, the velocity becomes lower when the water enters the volute spiral. This intense velocity difference at the impeller-volute boundary possibly affects the oil drops as well, forcing them to deform and break up, as explained in section 3.2. In addition, Fig. 10b confirms that the water – and, consequently, the oil drops – tend to circulate throughout the volute rather than exiting the pump stage. Once again, the PIV results are consistent with the observations from the HSI images.

Similar velocity fields were obtained for N = 900 rpm and Qw = 150 kg/h. Thus, the analysis made for N = 600 rpm in Fig. 10 is also valid for other operating conditions. For low flow rates close to shut-off, the water flow field is characterized by the presence of distorted velocity profiles, in addition to vortices and zones with reverse flow formed on the left side of the impeller, where the channels are next to the solid walls that compose the beginning of the volute, with the smallest spiral radii. Such a complex water flow probably explains the accumulation of oil drops observed in Figs. 8 and 9. The continuous phase tends to become "blocked" as the impeller channels rotate near the left side of the pump stage. Therefore, the dispersed phase would experience the same condition too.

The investigation was finally extended to N = 300 rpm. The spatial distribution of the average velocity, $\vec{u}$, and velocity fluctuations in the horizontal direction, u'_x, in the transparent pump stage are presented in Fig. 11 and Fig. 12, respectively. As explained in section 2.2, these PIV measurements were conducted for a single-phase water flow.

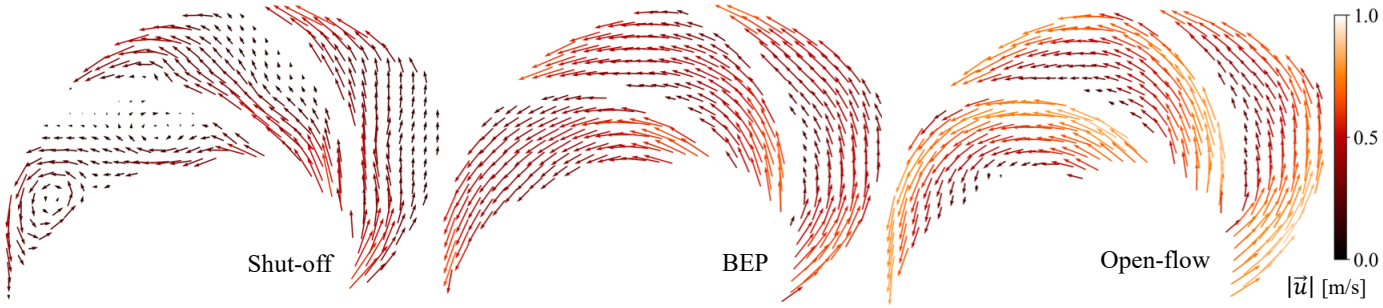

Fig. 11 - Average water velocity fields, at N = 300 rpm and Qw = [0, 750, 1100] kg/h or Qw = [0.0, 1.0, 1.5] Q_{BEP}.

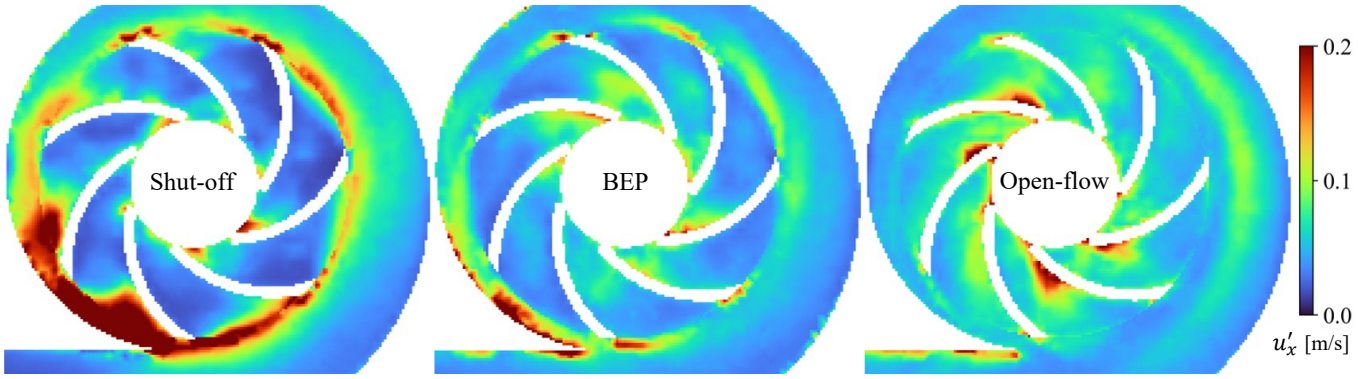

Fig. 12 - Water velocity fluctuations in horizontal direction, at N = 300 rpm and Qw = [0, 750, 1100] kg/h or Qw = [0.0, 1.0, 1.5] Q_{BEP}. The measurements were performed for a single-phase water flow without oil injection.

The flow field is complex when the pump operates at the shut-off point, with large velocity fluctuations in the impeller-volute region, where turbulence is thus expected to be very intense. This is exactly the region where the dispersed drops usually deform and break-up. Therefore, these results corroborate the observations made in section 3.2, especially in Fig. 3. The characteristics of the continuous phase are favorable to the fragmentation of the dispersed phase, which leads to the formation of emulsions in the pump stage.

The water flow becomes homogeneous and well-behaved at the BEP. Hence, the motion of the dispersed oil drops is expected to be more uniform, in agreement with the flow image of Fig. 4-left. In addition, regions with significant velocity fluctuations are identified at the tips of the impeller blades, where turbulence in the water phase possibly causes the oil drops to deform and break-up. The findings are congruent with the observations of Figs. 5 and 6 as well, in the scope of two-phase o/w dispersions.

At the open-flow condition, the magnitudes of the average velocity vectors become higher on the suction side of the blades. Inversely, the velocity fluctuations are more intense on the pressure surface of the blades. The irregular water velocity profile probably leads the dispersed oil drops to move from the suction to the pressure blade inside each channel. This fact would explain the agglomeration of oil drops in the vicinity of the pressure blades, as shown in Fig. 4-right, for example.

4. CONCLUSIONS

The present manuscript reports a set of results on the experimental investigation of two-phase oil-water dispersions in the impeller and volute of a transparent electrical submersible pump prototype. The tests were performed at UNICAMP, in Brazil, where HSI and PIV were used as flow visualization techniques. Flow patterns were qualitatively analyzed from the observation of the flow images. Oil drop fragmentation events were detected and associated with the formation of emulsions. The accumulation of oil drops within the impeller channels at low water flow rates was another phenomenon investigated. The most relevant observations include the following:

- When the water flow rate is low, $Qw < 0.1\ Q_{BEP}$, or the flow rate ratio is high, $\beta > 10.0\%$, the oil drops begin to accumulate in the impeller, which promotes the formation of a "concentrated drops" flow pattern. The forces acting on the drops are insufficient to guide them to the impeller outlet. Besides, the accumulation is a consequence of the water flow morphology, which is characterized by the presence of vortices and other structures in partially blocked channels. Breakage events occur predominantly on the boundary between impeller (moving part) and volute (stationary part), where the water velocity undergoes a significant discontinuity. This region is also associated with intense turbulence caused by velocity fluctuations in the continuous phase flow. From successive breakage events, there is the generation of an emulsion, which acquires a turbid and whitish appearance after a few seconds of oil injection in the pump stage.
- At the flow rate corresponding to BEP, $Qw \approx Q_{BEP}$, the water velocity field is well organized, thus the oil drops are evenly distributed in the entire pump stage. Thus, when the flow rate ratio is low, $\beta \approx 1.0\%$, the oil drops acquire an elliptical shape and become arranged in a "dispersed drops" flow pattern. Breakage events are detected at the tips of the blades on the impeller-volute boundary. Furthermore, many drops experience fragmentation when passing through the volute tongue region, where shear stress is expected to be high.
- The water phase continues influencing the oil phase even when the water flow rate is higher. At the open-flow, $Qw = 1.5\ Q_{BEP}$, the velocity profiles become irregular as the water flow undergoes a deviation in the channels. For $\beta \approx 1.0\%$, this fact causes the oil drops to migrate from the suction to the pressure surface of the blades. This situation tends to change the spatial distribution of the dispersed drops in the pump stage. Once again, the measurements performed with PIV corroborate the observations made with HSI.

This study based of flow visualization expands the literature on the behavior of two-phase liquid-liquid mixtures in pump impellers and diffusers. The main motivation for this research is the problems faced by the petroleum industry when using centrifugal pumps such as the ESP. The observations made with HSI and PIV in this manuscript are currently being used by other researchers at the same research group to the proposition and improvement of phenomenological models related to pump performance and effective viscosity. The findings are also important for the validation of numerical simulations, which often rely on turbulence models that cannot fully reproduce the real complex flows that take place in turbomachines.

As a continuity of this study, the comparison between water and oil is now being further explored. The PIV method is being adopted to visualize two-phase flows as well, for a complete analysis of how the presence of oil drops influence the water flow and vice-versa. Besides, in the near future, the experiments will be repeated with the inverted emulsion, i.e., water-in-oil (w/o) type, which is more representative of the emulsions pumped with real ESP in actual oil fields.

NOMENCLATURE

N	= Impeller rotational speed	(rpm)	V_R	= Oil drop radial velocity	(m/s)
ω	= Impeller angular speed	(rad/s)	V_θ	= Oil drop circumferential velocity	(m/s)
Qo	= Oil flow rate	(g/s)	$\vec{V}$	= Oil drop velocity vector	(m/s)
Qw	= Water flow rate	(kg/h)	$\vec{u}$	= Water relative velocity vector	(m/s)
Q_{BEP}	= Water flow rate at the BEP	(kg/h)	$\vec{U}$	= Water absolute velocity vector	(m/s)
P	= Absolute static pressure	(Pa)	u'	= Water velocity fluctuations	(m/s)
DP	= Differential static pressure	(Pa)	u'_x	= u' in the horizontal (x) direction	(m/s)
T	= Fluid temperature	(°C)	Mo	= Mass of oil injected in the pump	(kg)
ρ	= Fluid density	(kg/m³)	Mw	= Mass of water in the pump stage	(kg)
μ	= Fluid viscosity	(Pa.s)	λ	= Mass fraction	(-)
R	= Radial position	(m)	β	= Flow rate ratio	(-)
θ	= Circumferential position	(rad)	t	= Time or instant of time	(s)

ACKNOWLEDGEMENTS

We gratefully acknowledge the support of EPIC - Energy Production Innovation Center, hosted by the University of Campinas (UNICAMP) and sponsored by Equinor Brazil and FAPESP - The Sao Paulo Research Foundation (Process Number 2017/15736-3). We also thank FAPESP for providing the PIV system used in this research through the Multi-User Equipment program (Process Number 2019/20870-6). We acknowledge the support of ANP (Brazil's National Oil, Natural Gas and Biofuels Agency) through the R&D levy regulation. Acknowledgments are also extended to Center for Energy and Petroleum Studies (CEPETRO), School of Mechanical Engineering (FEM), and ALFA Research Group.

REFERENCES

Bremner, C., Harris, G., Kosmala, A., Nicholson, B., Ollre, A., Pearcy, M., Salmas, C.J., Solanki, S.C., 2006. Evolving technologies: electrical submersible pumps. *Oilfield Review*, pp. 30–43.

Bulgarelli, N.A.V., Biazussi, J.L., Monte Verde, W., Castro, M.S., Bannwart, A.C., 2020a. Experimental study of phase inversion phenomena in electrical submersible pumps under oil/water flow. *J. Offshore Mech. Arct. Eng.*, *142*, 041402.

Bulgarelli, N.A.V., Biazussi, J.L., Monte Verde, W., Perles, C.E., Castro, M.S., Bannwart, A.C., 2020b. Experimental investigation on the performance of electrical submersible pump operating with unstable water/oil emulsions. *J. Petrol. Sci. Eng.*, *197*, 107900.

Bulgarelli, N.A.V., Biazussi, J.L., Monte Verde, W., Perles, C.E., Castro, M.S., Bannwart, A.C., 2021. Relative viscosity model for oil/water stable emulsion flow within electrical submersible pumps. *Chem. Eng. Sci.*, *245*, 116827.

Cerqueira, R.F.L., Perissinotto, R.M., Monte Verde, W., Biazussi, J.L., Castro, M.S., Bannwart, A.C. Development and assessment of a particle tracking velocimetry (PTV) measurement technique for the experimental investigation of oil drops behavior in dispersed oil-water two-phase flow within a centrifugal pump impeller. *Int. J. Multiph. Flow*, under review (*no prelo*).

Cubas, J.M.C., Stel, H., Ofuchi, E.M., Neto, M.A.M., Morales, R.E.M., 2020. Visualization of two-phase gas-liquid flow in a radial centrifugal pump with a vaned diffuser. *J. Petrol. Sci. Eng.*, *187*, 106848.

Flatern, R., 2015. The Defining Series: Electrical Submersible Pumps. *Oilfield Review*, pp. 1–2.

Ibrahim, S.Y., Maloka, I.E., 2006. Emulsification of secondary oil/water dispersions using a centrifugal pump. *Petrol. Sci. Technol.*, *24*, pp. 513–522.

Keller, J., Blanco, E., Barrio, R., Parrondo, J., 2014. PIV measurements of the unsteady flow structures in a volute centrifugal pump at a high flow rate. *Exp. Fluids*, *55*, 1820.

Krause, N., Pap, E., Thévenin, D., 2006. Investigation of off-design conditions in a radial pump by using time-resolved-PIV. Lisbon: *13th International Symposium on Applications of Laser Techniques to Fluid Mechanics*.

Li, X., Chen, B., Luo, X., Zhu, Z., 2020. Effects of flow pattern on hydraulic performance and energy conversion characterization in a centrifugal pump. *Renew. Energy*, *151*, pp. 475–487.

Liu, X-D., Liu, Z-Q., Zhong, Q., Li, Y-J., Yang, W., 2021. Experimental investigation of relative velocity field based on image rotation method in a pump impeller. *Flow Meas. Instrum*., *82*, 102061.

Mansour, M., Parikh, T., Engel, S., Wunderlich, B., Thévenin, D., 2019. Investigation on the influence of an inducer on the transport of single and two-phase air-water flows by centrifugal pumps. Houston, Texas: *48th Turbomachinery and 35th Pump Symposia*.

Monte Verde, W., Biazussi, J.L., Sassim, N.A., Bannwart, A.C., 2017. Experimental study of gas-liquid two-phase flow patterns within centrifugal pumps impellers. *Exp. Therm. Fluid Sci.*, *85*, pp. 37–51.

Morales, R., Pereyra, E., Wang, S., Shoham, O., 2012. Droplet formation through centrifugal pumps for oil-in-water dispersions. *SPE 18*, pp. 172–178.

Morrison, G., Chen, Y., Steck, D., Chen, Y., Bai, C., Patil, A., 2017. Effect of gas presence on erosive wear of split-vane electrical submersible pump. Houston, Texas: *46th Turbomachinery and 33th Pump Symposia*.

Pedersen, N., Larsen, P.S., Jacobsen, C.B., 2003. Flow in a centrifugal pump impeller at design and off-design conditions - Part I: particle image velocimetry (PIV) and laser doppler velocimetry (LDV) measurements. *J. Fluids Eng., 125*, pp. 61–72.

Perissinotto, R.M., Monte Verde, W., Castro, M.S., Biazussi, J.L., Estevam, V., Bannwart, A.C., 2019. Experimental investigation of oil drops behavior in dispersed oil-water two-phase flow within a centrifugal pump impeller. *Exp. Therm. Fluid Sci.*, *105*, pp. 11–26.

Perissinotto, R.M., Monte Verde, W., Perles, C.E., Biazussi, J.L., Castro, M.S., Bannwart, A.C., 2020. Experimental analysis on the behavior of water drops dispersed in oil within a centrifugal pump impeller. *Exp. Therm. Fluid Sci.*, *112*, 109969.

Perissinotto, R.M., Monte Verde, W., Biazussi, J.L., Bulgarelli, N.A.V., Fonseca, W.D.P., Castro, M.S., Franklin, E.M., Bannwart, A.C., 2021. Flow visualization in centrifugal pumps: A review of methods and experimental studies. *J. Petrol. Sci. Eng.*, *203*, 108582.

Perissinotto, R.M., Fonseca, W.D.P., Cerqueira, R.F.L., Monte Verde, W., Biazussi, J.L., Castro, M.S., Bannwart, A.C., 2022. Development of a transparent pump prototype for flow visualization purposes. *Rio Oil & Gas Expo and Conference, Brazilian Petroleum and Gas Institute*.

Raffel, M., Willert, C., Wereley, S., Kompenhans, J., 2007. *Particle Image Velocimetry: A Practical Guide*, 2nd ed, Berlin: Springer.

Schmitt, P., Sibirtsev, S., Hlawitschka, M.W., Styn, R., Jupke, A., Bart, H.J., 2021. Droplet size distribution of liquid-liquid dispersions in centrifugal pumps. *Chem. Ing. Tech.*, *93*.

Shao, C., Li, C., Zhou, J., 2018. Experimental investigation of flow patterns and external performance of a centrifugal pump that transports gas-liquid two-phase mixtures. *Int. J. Heat Fluid Fl.*, *71*, pp. 460–469.

Shi, B., Zhou, K., Pan, J., Zhang, X., Ying, R., Wu, L., Zhang, Y., 2021. PIV test of the flow field of a centrifugal pump with four types of impeller blades. *J. Mech.*, *37*, pp. 192–204.

Stel, H., Ofuchi, E.M., Sabino, R.H.G., Ancajima, F.C., Bertoldi, D., Neto, M.A.M., Morales, R.E.M., 2019. Investigation of the motion of bubbles in a centrifugal pump impeller. *J. Fluids Eng.*, *141*, 031203.

Takacs, G., 2017. *Electrical Submersible Pumps Manual: Design, Operations, and Maintenance*, 2nd ed., Oxford: GPP.

Thielicke, W., Sonntag, R., 2021. Particle image velocimetry for MATLAB: Accuracy and enhanced algorithms in PIVlab. *Journal of Open Research Software*, *9*, pp. 12.

U.S. Energy Information Administration: *Frequently Asked Questions*. Retrieved on November, 10th, 2021, from https://www.eia.gov/tools/faqs/faq. php?id=709&t=6 (web address).

Valdés, J.P., Asuaje, M., Ratkovich, N., 2020. Study of an ESP's performance handling liquid-liquid flow and unstable O-W emulsions. Part I: Experimental. *Chem. Eng. Sci*., *223*, 115726.

Zhao, L., Chang, Z., Zhang, Z., Huang, R., He, D., 2021. Visualization of gas-liquid flow pattern in a centrifugal pump impeller and its influence on the pump performance. *Measurement: Sensors*, *13*, 100033.